JACS
JOURNAL OF THE AMERICAN CHEMICAL SOCIETY
Communication
pubs.acs.org/JACS

Increasing the Band Gap of Iron Pyrite by Alloying with Oxygen

Jun Hu,[†] Yanning Zhang,[†] Matt Law,[‡] and Ruqian Wu*[,†]

[†]Department of Physics and Astronomy, University of California, Irvine, California 92697-4575, United States

[‡]Department of Chemistry and Department of Chemical Engineering and Materials Science, University of California, Irvine, California 92697, United States

Supporting Information

ABSTRACT: Systematic density functional theory studies and model analyses have been used to show that the band gap of iron pyrite (FeS_2) can be increased from ∼1.0 to 1.2−1.3 eV by replacing ∼10% of the sulfur atoms with oxygen atoms (i.e., ∼10% O_S impurities). O_S formation is exothermic, and the oxygen atoms tend to avoid O−O dimerization, which favors the structural stability of homogeneous $FeS_{2-x}O_x$ alloys and frustrates phase separation into FeS_2 and iron oxides. With an ideal band gap, absence of O_S-induced gap states, high optical absorptivity, and low electron effective mass, $FeS_{2-x}O_x$ alloys are promising for the development of pyrite-based heterojunction solar cells that feature large photovoltages and high device efficiencies.

Iron pyrite (FeS_2) is a promising photovoltaic material because of its strong light absorption ($\alpha > 10^5$ cm^{-1} for $h\nu >$ 1.3−1.4 eV), sufficient minority carrier diffusion length (100−1000 nm), and essentially infinite elemental abundance.[1−6] Pyrite photoelectrochemical and solid-state Schottky solar cells have shown large short-circuit current densities (30−42 mA cm^{-2}) and quantum efficiencies (up to 90%).[7,8] However, the open-circuit voltage (V_{OC}) of pyrite cells is low [$V_{OC} \leq 0.2$ eV, which is less than ∼20% of the band gap (E_g) of ∼0.95 eV].[3] The cause of the abnormally low V_{OC} of pyrite devices remains unclear and has been the subject of several recent investigations.[9−12] The band gap of pyrite is also somewhat narrow for optimal photovoltaic applications according to the Shockley−Queisser theory.[13] Therefore, identifying practical ways to increase the pyrite band gap is of interest for the development of pyrite-based photovoltaics. Substituting cations or anions with isovalent elements or compensated dimers is a widely used approach for modifying the band gaps of other semiconductors, including III−V materials[14] and ternary ABC_2 chalcopyrite compounds.[15] A recent density functional theory (DFT) study by Sun and Ceder[16] found that the band gap of pyrite can be increased slightly by replacing some Fe by Ru or Os to form $Fe_{1-x}Ru_xS_2$ and $Fe_{1-x}Os_xS_2$ compounds. However, this approach is limited by the overall weakness of the effect (E_g increases by only ∼0.1 eV even at x = 0.5) and the low solubility of Ru and Os in pyrite. These authors also investigated $Fe_{1-x}Zn_xS_2$ alloys but found that substitutional zinc (Zn_{Fe}) results in significant band-gap narrowing for x up to 0.5 (i.e., 50% Zn_{Fe}), in spite of the large band gap of pyrite ZnS_2 itself (∼2.5 eV).[17] Our own calculations on $Fe_{1-x}Zn_xS_2$ alloys are in good agreement with the results of Sun and Ceder (see Figure S1 in the Supporting Information). We have found that substitution of Zn for Fe produces gap states and new valence bands above the Fe t_{2g} bands of pyrite, leading to a narrowed band gap at large Zn_{Fe} concentrations (Figure S2). The unexpected ineffectiveness of cation alloying calls for a new approach to increase the band gap of iron pyrite.

In this work, we used systematic DFT calculations to investigate the effect of large concentrations of substitutional oxygen (O_S) on the band gap and other electronic and optical properties of pyrite. We found that O_S concentrations of ∼10% increase E_g to 1.2−1.5 eV (depending on the exact spatial distribution of the O_S centers) without producing electronic states within the band gap. The resulting $FeS_{2-x}O_x$ ($x \approx 0.2$) alloys are thermodynamically stable, retain the relatively small electron effective mass of pure pyrite, and show better light absorption than pyrite itself in the near-IR region of the spectrum. Oxygen-alloyed pyrite may therefore be promising for the fabrication of pyrite solar cells with larger V_{OC} values, provided that synthetic schemes that avoid the phase separation of iron oxides can be developed.

To rationally increase the band gap of pyrite, it is essential to understand the nature of the electronic states at its valence band maximum (VBM) and conduction band minimum (CBM). Pyrite adopts a NaCl-like structure (space group $Pa\bar{3}$)[18] with a face-centered cubic sublattice of Fe^{2+} cations and S_2^{2-} dimers at the anion positions (Figure 1a). Each Fe ion is coordinated to six S ions, and each S ion is located at the center of a tetrahedron consisting of another S atom and three Fe atoms. The 3d orbitals of Fe are split into t_{2g} and e_g groups in the approximately O_h local symmetry, while the 3p orbitals of S are split into four groups in the C_{3v} symmetry (Figure 1b). The actual energy sequence of the Fe and S states of bulk pyrite is shown in the calculated band structure in Figure 1c. The valence bands originate almost completely from the Fe t_{2g} orbitals, showing little Fe−S hybridization within 1 eV of the VBM. In contrast, Fe e_g and S ppσ* orbitals strongly hybridize in the conduction bands, as indicated by the rapid changes in the Fe and S weights for bands ∼3 eV above the VBM in Figure 1c. It is important to note that the bottom of the S ppσ* band extends ∼1 eV below the Fe e_g bands, meaning that the CBM of pyrite is almost purely S ppσ* in character (98%). This can be seen more clearly from the isosurfaces of the single-state charge density of the CBM (Figure 1d), which appears as a network of S ppσ* orbitals.

Received: June 9, 2012
Published: July 24, 2012

   dx.doi.org/10.1021/ja3053464 | J. Am. Chem. Soc. 2012, 134, 13216−13219

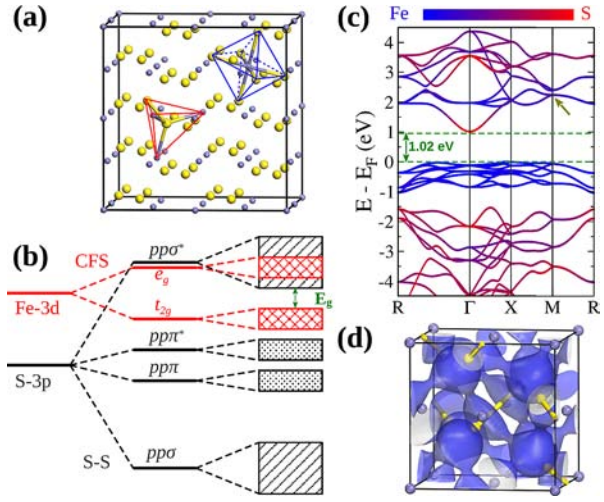

Figure 1. Crystal structure and electronic properties of bulk iron pyrite. (a) 2 × 2 × 2 supercell of bulk pyrite (96 atoms). The yellow and purple spheres denote S and Fe atoms, respectively. The local symmetries around the Fe and S atoms are indicated by the blue octahedron and the red tetrahedron, respectively. (b) Sketch of the energy diagram for the Fe 3d and S 3p orbitals of bulk pyrite under the influences of crystal-field splitting (CFS) and S−S dimerization. The green arrow denotes the band gap (E_g). (c) Band structure of bulk pyrite with a color scale indicating the contributions from Fe and S atoms. Atomic contributions were computed by projecting the Bloch wave functions of pyrite into atomic orbitals of Fe and S atoms. It should be noted that the conduction band minimum (CBM) consists almost completely of S ppσ* orbitals, as shown also in (b). The horizontal dashed green lines indicate the energy positions of the valence band maximum (VBM) and the CBM. The brown arrow marks the degenerate Fe e_g levels that split in the presence of O_S, as highlighted in Figure 2. (d) Single-state charge density of the CBM at 0.016 e/Å^3 for a conventional pyrite unit cell.

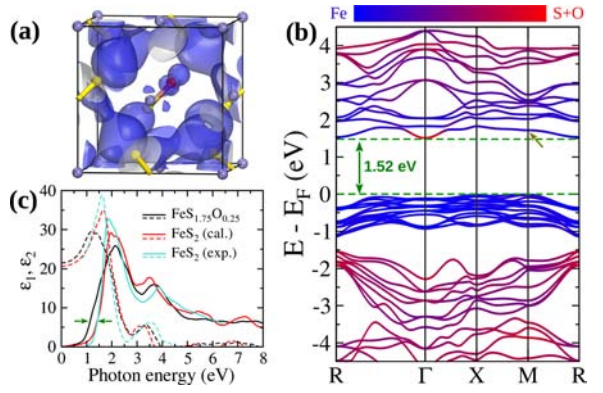

Figure 2. Electronic and optical properties of $FeS_{1.75}O_{0.25}$ (12.5% O_S) using the most ordered configuration. (a) Unit cell (Fe_4S_7O) and the isosurfaces of the single-state charge density of the new CBM. The red, yellow, and purple spheres denote O, S, and Fe atoms, respectively. (b) Band structure, with a color scale indicating the contributions from the cation (Fe) and the anions (S and O). The horizontal dashed green lines indicate the energy positions of the VBM and CBM. The brown arrow marks the split Fe e_g level at the M point. (c) Calculated dielectric functions ($\boldsymbol{\varepsilon} = \varepsilon_1 + i\varepsilon_2$) of $FeS_{1.75}O_{0.25}$ (black lines) and bulk pyrite (red lines),[21] accompanied with experimental data for bulk pyrite.[22] Dashed and solid curves represent ε_1 and ε_2, respectively. Green arrows highlight the downward shift of the optical absorption edge due to the oxygen alloying effect.

With this picture in mind, one may increase the E_g of pyrite by reducing the bandwidth of the S ppσ* bands to lift the CBM toward the Fe e_g bands. One proposal to achieve this, as reported by Sun and Ceder,[16] would be to expand the unit cell by incorporating large isovalent cations such as Ru and Os. However, the effect of strain on E_g is very small; for example, E_g is larger by only ∼0.1 eV at Ru or Os concentrations as high as 50%. A more direct and effective approach is to reduce the average hopping integral within the S ppσ* orbital network by replacing a fraction of the sulfur anions with smaller oxygen anions. Because oxygen 2p orbitals are smaller than sulfur 3p orbitals, oxygen anions would be expected to act as pinch points in the S ppσ* network and thereby reduce its bandwidth, widening the pyrite band gap. In our recent studies,[19] we reported that the binding energy of oxygen on a sulfur site (O_S) is ∼0.16 eV larger than that of sulfur on a sulfur site (S_S), showing that oxygen should be readily incorporated into pyrite. That same work also demonstrated that O_S impurities at a concentration of 1.6 atom % increase E_g slightly (by 0.04 eV) without producing electronic states within the band gap to act as traps or recombination centers. From the calculated formation energies, Sun et al.[20] also showed that neutral O_S are the most dominant impurities in pyrite, whereas the population of interstitial O atoms is negligible.

To determine the effect of high O_S concentrations on the band gap of pyrite, we first analyzed the most ordered possible structure of $FeS_{1.75}O_{0.25}$ using a Fe_4S_7O conventional cubic unit cell with 12.5% O_S, as depicted in Figure 2a. Figure 2b shows the band structure of this hypothetical $FeS_{1.75}O_{0.25}$ alloy. From a comparison with the band structure of bulk pyrite in Figure 1c, it is evident that the CBM of the $FeS_{1.75}O_{0.25}$ alloy shifts upward toward the Fe e_g bands, increasing the band gap to 1.52 eV without introducing gap states. This indicates that replacing sulfur with isovalent oxygen is indeed a more promising strategy than cation substitution for modifying the pyrite band gap. From the single-state electron density plot in Figure 2a for the new CBM at the Γ point, we observe that the CBM still originates from the S ppσ* states, but the continuous S ppσ* network of pure pyrite is disrupted around the O−S dimers because O_S has a more localized wave function and a different potential than the rest of the anion sublattice.[23] These features of O_S are ideal for reducing the S ppσ* bandwidth and widening the pyrite band gap. The effective mass of carriers at the new CBM is $0.67m_e$ (compared with $0.44m_e$ for pure pyrite), so the electron mobility of $FeS_{1.75}O_{0.25}$ should be similar to that of pyrite given comparable scattering times for electrons. Meanwhile, the VBM shifts to the M point, and the effective hole mass becomes $1.44m_e$, which is comparable to that of pure pyrite ($1.23-1.98m_e$, depending on crystal direction).[19]

It is worth pointing out that the orbital overlap and hence the optical transitions between Fe t_{2g} states in the valence bands and S ppσ* states in the conduction bands are negligible. Thus, the optical absorption of pyrite originates mainly from electric dipole transitions between Fe t_{2g} and Fe e_g states, with the latter mixed with some S p and Fe p states to fulfill the optical selection rules. The calculated dielectric functions in Figure 2c indicate that most of the optical absorption peaks of pyrite are not significantly affected by the upward shift of the S ppσ* bands in $FeS_{1.75}O_{0.25}$. Interestingly, the presence of O_S makes the optical absorption threshold shift downward by ∼0.4 eV, as highlighted by the green arrows in Figure 2c. Therefore, $FeS_{2-x}O_x$ alloys are actually stronger light absorbers than pure pyrite, despite their larger band gaps. The reliability of this

dx.doi.org/10.1021/ja3053464 | J. Am. Chem. Soc. 2012, 134, 13216−13219

prediction is attested by the good agreement between the calculated dielectric functions and recent spectroscopic ellipsometry measurements on pyrite single crystals.[22] Through analysis of momentum matrix elements, we found that the optical absorption edges of both pyrite and $FeS_{1.75}O_{0.25}$ result mainly from electric dipole transitions between the highest Fe t_{2g} valence states and the lowest Fe e_g states around the M point.[22] The enhanced optical absorption of $FeS_{1.75}O_{0.25}$ in the near-IR region can be traced to the splitting of the fourfold-degenerate Fe e_g bands that are marked by the brown arrows in Figures 1c and 2b. Because of the reduction of local symmetry around Fe, the Fe e_g bands of pure pyrite split into two branches in $FeS_{1.75}O_{0.25}$ at ~2.2 eV above E_F at the M point, with one branch dropping by 0.4 eV. Therefore, a high concentration of O_S in pyrite not only increases the band gap but may also further enhance its overall optical absorptivity.

Now we turn to the effect of the O_S concentration on the band gap and other pertinent properties of $FeS_{2-x}O_x$ alloys with x up to 1.0 (50% O_S) using 2 × 2 × 2 supercells (96 atoms). The main results of these systematic studies are shown in Figure 3a. The most striking finding is the strong monotonic increase of E_g with increasing x, up to E_g = 1.88 eV for x = 1.0. We see that the lattice constant decreases as x increases because of the smaller size of oxygen compared with sulfur. Meanwhile, the formation enthalpy [defined as the difference of total energies, i.e., $\Delta H_f = E_{FeS_{2-x}O_x} - E_{FeS_2} - (x/2)E_{O_2} + (x/8)E_{S_8}$] decreases with increasing x, indicating that oxygen substitution in pyrite is energetically favorable (as expected). If we further consider the potential for iron oxide precipitation at large oxygen loadings, incorporating oxygen into pyrite at concentrations above 15−20% is probably impractical. However, we believe that ~10% O_S alloying without phase separation may be experimentally feasible through kinetic trapping of the alloy during synthesis.[4,24]

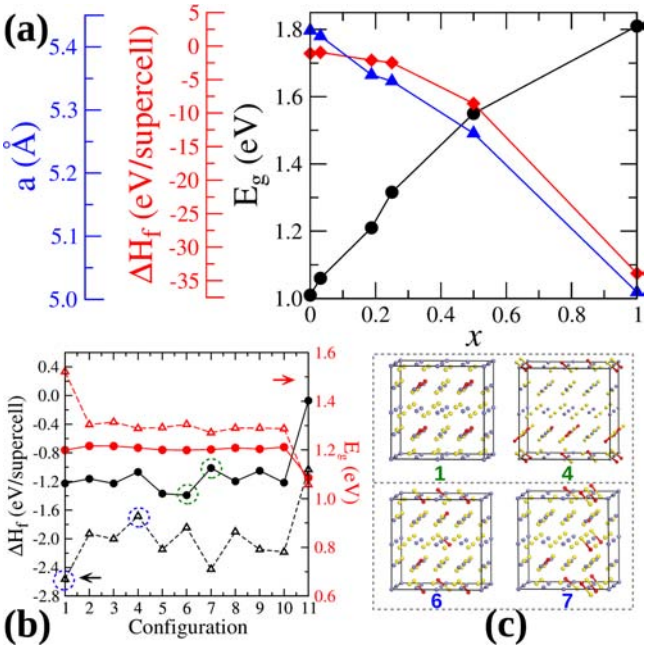

Figure 3. Physical attributes and structural features of $FeS_{2-x}O_x$ alloys. (a) Lattice constant, formation enthalpy, and band gap as functions of x. (b) ΔH_f and E_g of $FeS_{1.75}O_{0.25}$ (open triangles) and $FeS_{1.8125}O_{0.1875}$ (solid circles) calculated for various O_S configurations. Configurations 1−10 contain only S−S and S−O dimers arranged in different patterns, while configuration 11 contains one O−O dimer. Configuration 1 of the $FeS_{1.75}O_{0.25}$ alloy is equivalent to the evenly distributed O_S case of Figure 2a. (c) Selected atomic structures of (top) $FeS_{1.75}O_{0.25}$ and (bottom) $FeS_{1.8125}O_{0.1875}$ alloys with the lowest and highest enthalpies, as indicated by the dashed circles in (b) for each stoichiometry. Numbers denote the corresponding structures in (b). The red, yellow, and purple spheres represent O, S, and Fe atoms, respectively.

We also tested the robustness of the E_g increase for different O_S configurations. We studied 11 atomic configurations of $FeS_{2-x}O_x$ alloys (full details are shown in Figures S3 and S4) by randomly replacing six sulfur atoms (for x = 0.1875, or 9.4% O_S) or eight sulfur atoms (for x = 0.25, or 12.5% O_S) with oxygen atoms in the 2 × 2 × 2 supercell. For both concentrations, configurations 1−10 contained only S−S and S−O dimers, while configuration 11 included one O−O dimer to evaluate the likelihood of O−O dimerization in pyrite. As shown in Figure 3b, configuration 11 has a substantially more positive formation enthalpy than configurations 1−10 at both O_S concentrations, by as much as 1.1 eV per O−O dimer. Therefore, the equilibrium concentration of O−O dimers should be lower than that of O−S dimers by a factor of 10^{13}−10^{14} at T = 400−500 K according to the Boltzmann equation. Furthermore, several of the results in Figure 3b show that O_S centers tend to be distributed uniformly in the pyrite lattice. First, the most ordered (uniform) configuration of $FeS_{1.75}O_{0.25}$ (configuration 1) is more stable than configurations 2−10 by 0.4−0.8 eV per supercell (or 12−28 meV per formula unit). Second, the less uniform distribution of $FeS_{1.8125}O_{0.1875}$ (configuration 7) is ~0.1 eV higher in energy than configuration 6. Significantly, the band gap is insensitive to the spatial configuration of the O−S dimers when O−O dimerization is excluded. E_g is ~1.3 eV for configurations 2−10 of $FeS_{1.75}O_{0.25}$ and ~1.2 eV for configurations 1−10 of $FeS_{1.8125}O_{0.1875}$. This insensitivity of E_g to the O−S configuration increases the chance of synthesizing $FeS_{2-x}O_x$ films with stable band gaps larger than 1.2 eV using appropriate experimental conditions.

In summary, we have found that substituting oxygen for sulfur is an effective way to increase the band gap of iron pyrite while avoiding gap states and maintaining the favorable electrical and optical properties of pure pyrite. O_S alloying at ~10% reduces the width of the sulfur ppσ* band and raises the CBM by 0.2−0.3 eV regardless of the exact spatial distribution of the O_S centers. Our results show the promise of fabricating pyrite absorber layers with optimum band gaps for photovoltaic applications (1.2−1.3 eV). Experimental verification of this important prediction is in progress in our laboratories.

■ ASSOCIATED CONTENT

Supporting Information

Computational methods, results for $Fe_{1-x}Zn_xS_2$ alloys, and atomic structures of $FeS_{2-x}O_x$ alloys. This material is available free of charge via the Internet at http://pubs.acs.org.

■ AUTHOR INFORMATION

Corresponding Author

wur@uci.edu

Notes

The authors declare no competing financial interest.

■ ACKNOWLEDGMENTS

We thank the NSF SOLAR Program (Award CHE-1035218) and the UCI School of Physical Sciences Center for Solar Energy for support of this work. Calculations were performed on parallel computers at NERSC and at NSF supercomputer centers.

■ REFERENCES

(1) Schlegel, A.; Wachter, P. *J. Phys. C: Solid State Phys.* **1976**, *9*, 3363.
(2) Altermatt, P. P.; Kiesewetter, T.; Ellmer, K.; Tributsch, H. *Sol. Energy Mater. Sol. Cells* **2002**, *71*, 181.
(3) Ennaoui, A.; Tributsch, H. *Sol. Energy Mater.* **1986**, *14*, 461.
(4) Smestad, G.; Ennaoui, A.; Fiechter, S.; Tributsch, H.; Hofmann, W. K.; Birkholz, M.; Kautek, W. *Sol. Energy Mater.* **1990**, *20*, 149.
(5) Wadia, C.; Alivisatos, A. P.; Kammen, D. M. *Environ. Sci. Technol.* **2009**, *43*, 2072.
(6) Ennaoui, A.; Fiechter, S.; Pettenkofer, Ch.; Alonso-Vante, N.; Büker, K.; Bronold, M.; Höpfner, Ch.; Tributsch, H. *Sol. Energy Mater. Sol. Cells* **1993**, *29*, 289.
(7) Ennaoui, A.; Fiechter, S.; Jaegermann, W.; Tributsch, H. *J. Electrochem. Soc.* **1986**, *133*, 97.
(8) Büker, K.; Alonso-Vante, N.; Tributsch, H. *J. Appl. Phys.* **1992**, *72*, 5721.
(9) Sun, R.; Chan, M. K. Y.; Ceder, G. *Phys. Rev. B* **2011**, *83*, 235311.
(10) Yu, L.; Lany, S.; Kykyneshi, R.; Jieratum, V.; Ravichandran, R.; Pelatt, B.; Altschul, E.; Platt, H. A. S.; Wager, J. F.; Keszler, D. A.; Zunger, A. *Adv. Energy Mater.* **2011**, *1*, 748.
(11) Zhang, Y. N.; Hu, J.; Law, M.; Wu, R. Q. *Phys. Rev. B* **2012**, *85*, 085314.
(12) Berry, N.; Cheng, M.; Perkins, C. L.; Limpinsel, M.; Hemminger, J. C.; Law, M. *Adv. Energy Mater.* **2012**, DOI: 10.1002/aenm.201200043.
(13) Shockley, W.; Queisser, H. *J. Appl. Phys.* **1961**, *32*, 510.
(14) Geller, C. B.; Wolf, W.; Picozzi, S.; Continenza, A.; Asahi, R.; Mannstadt, W.; Freeman, A. J.; Wimmer, E. *Appl. Phys. Lett.* **2001**, *79*, 368.
(15) Jaffe, J. E.; Zunger, A. *Phys. Rev. B* **1983**, *27*, 5176.
(16) Sun, R.; Ceder, G. *Phys. Rev. B* **2011**, *84*, 245211.
(17) Jarrett, H. S.; Cloud, W. H.; Bouchard, R. J.; Butler, S. R.; Frederick, C. G.; Gillson, J. L. *Phys. Rev. Lett.* **1968**, *21*, 617.
(18) Bayliss, P. *Am. Mineral.* **1989**, *74*, 1168.
(19) Hu, J.; Zhang, Y. N.; Law, M.; Wu, R. Q. *Phys. Rev. B* **2012**, *85*, 085203.
(20) Sun, R.; Chan, M. K. Y.; Kang, S. Y.; Ceder, G. *Phys. Rev. B* **2011**, *84*, 035212.
(21) The dielectric functions were calculated without the *U* correction term in the generalized gradient approximation for better comparison with the experimental data.
(22) Choi, S., unpublished data. The experimental data was taken from natural iron pyrite crystal at room temperature.
(23) As discussed in ref 19, O−S dimers in pyrite are strongly polarized, with O atoms taking electrons from their Fe and S neighbors. Therefore, sulfur atoms in O−S dimers are different from those in S−S dimers, and the hybridization between orbitals in O−S dimers and S−S dimers is substantially reduced.
(24) For 9.4% O_S, the reactions $Fe_{32}S_{58}O_6 \rightarrow 28FeS_2 + 2Fe_2O_3 + S_2$ and $Fe_{32}S_{58}O_6 \rightarrow 28FeS_2 + 4FeO + O_2 + S_2$ release energies of 3.7 and 1.3 eV per supercell, respectively. In view of the energy costs of precipitation-induced lattice distortion as well as the preferential uniform distribution of O_S atoms in $FeS_{2-x}O_x$ alloys, the formation of Fe_2O_3 or FeO precipitates should be reasonably frustrated. It should be noted that the reaction energies depend on the choice of *U* for Fe_2O_3. Here we used U = 5.5 eV for the best fit of the band gap of Fe_2O_3 (2.2 eV).